



ELSEVIER

Available online at www.sciencedirect.com

SCIENCE @ DIRECT®

Optics Communications 236 (2004) 45–52

OPTICS
COMMUNICATIONS

www.elsevier.com/locate/optcom

Temporal processing with the Montgomery interferometer

Gladys Mínguez-Vega^a, Jürgen Jahns^{b,*}

^a *Departament de Ciències Experimentals, Universitat Jaume I, 12080 Castelló, Spain*

^b *FernUniversität Hagen, Optische Nachrichtentechnik, Universitätsstr. 27/PRG, 58084 Hagen, Germany*

Received 28 November 2003; received in revised form 3 March 2004; accepted 5 March 2004

Abstract

In this work, the strong interaction between the spatial and temporal frequencies is exploited by the Montgomery interferometer to process time-limited signals. With this objective and using the scalar diffraction theory, we identify the transfer function of the setup for the on-axis pulse plane wave. Moreover, in order to control the output complex field envelope, a linear and quadratic order Taylor approximation for the transfer function of each spatial frequency is performed. The potential applications of this device, the study of the validity of the approach and some numerical examples are also presented.

© 2004 Elsevier B.V. All rights reserved.

PACS: 41.85; 42.25; 42.40

Keywords: Diffraction; Spatio-temporal processing; Tapped delay-line filter; Pulse-shaping; Self-imaging; Short pulses

1. Introduction

The first report of the self-imaging phenomenon is due to Talbot [1]. Under the paraxial approximation, he observed that a laterally periodic object illuminated by a quasi-monochromatic plane wave replicates itself along the direction of propagation. The longitudinal period of the wave field is often referred to as the Talbot distance. Although lateral periodicity is a sufficient condition, it was not until 1967 when Montgomery described the necessary

and sufficient requirements for self-imaging. He found that the spatial frequencies of an object generating a self-imaging wave field – called “Montgomery object” after him – must be confined to well-defined radii [2]. 1D gratings and certain 2D gratings satisfy this constraint and constitute a subset of the Montgomery objects. A detailed overview of the first studies, mostly focussed on periodic structures, can be found in [3]. Applications of self-imaging in the spatial domain include Fourier transform spectroscopy [4,5], white-light free-space optical interconnection [6] and double-sided lithographic alignment [7].

Another application of the wave field replication is interferometry. Due to limited fabrication capabilities, only simple mask patterns were used

* Corresponding author. Tel.: +492331987340; fax: +492331987352.

E-mail address: jahns@fernuni-hagen.de (J. Jahns).

initially. Lohmann and Silva [8] suggested a Talbot interferometer for phase-gradient measurement. Indebetouw [9] used spatial filtering with a Fabry–Perot interferometer to experimentally demonstrate Montgomery self-imaging. Now, thanks to the improvement of technology in the fabrication of micro relief diffractive optical elements (DOEs) [10], both, high design flexibility and complex phase structures are accessible. Recently, a Montgomery interferometer with two phase-complementary computer-generated DOEs based on binary optics technology has been implemented [11]. This setup as well as its Talbot version were suggested as tapped delay-line filters for temporal signal processing [11,12].

In a tapped delay-line or transversal filter, see Fig. 1, an input signal is split into several branches, individually delayed and weighted and, finally, recombined. In the Montgomery interferometer, the beam splitting and beam recombination is done by the Montgomery objects. Meanwhile, the delay is the result of different optical paths corresponding to each spatial frequency in free-space propagation. This device is easy to assemble, has a relative low price and seems suitable for integration technology. Silica-based single-mode waveguides [13], acousto-optic devices [14], in-fiber Bragg gratings reflectors [15] and multimode interference coupler [16] among others, have also been proposed as tapped delay-lines.

Although time filters are very important in telecommunications research [17], the generation of a train of pulses, pulse-shaping and space-time conversion are just a few examples of the research subjects where the Montgomery interferometer

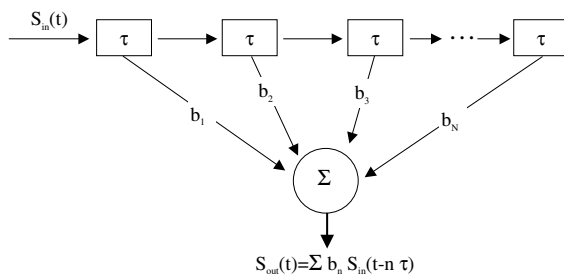


Fig. 1. Tapped delay-line filter with tap intervals τ and weighting elements b_n ($n = 1, 2, \dots, N$).

may participate with a novel physical approach. For a review of these topics, we suggest [18–20] and enclosed citations. In former pulse-shaping devices [21,22], only single spatial frequency structures (as kinoform gratings) are considered for building the temporal processing setup. This is the main difference with the Montgomery interferometer that takes advantage of the strong interaction between spatial and temporal frequencies to perform temporal processing. In fact, the Treacy grating pairs pulse compressor [21] can be understood as a particular case of the Montgomery interferometer.

All these matters encourage us to present, in this communication, an extensive theoretical analysis of the temporal behaviour of the Montgomery interferometer. First, we will review the background theory of narrowband signal propagation in linear optical systems. In a second step, we will calculate the transfer function of the Montgomery interferometer. Since for each spatial frequency the phase transfer function differs from the dispersion-free case of an ideal filter, a second- and third-order Taylor approximation will be performed. This enables us to study the delay of the envelope and its shape changes for each output pulse. In order to demonstrate the validity of this approach, we define a merit function that measures the goodness of the approximation and we include some numerical examples.

2. Propagation of bandwidth-limited signals in linear optical setups

In this section, we review some general aspects of temporal signals propagation [23,24]. We restrict ourselves to the temporal and spectral modifications of the pulse neglecting any possible changes of the output spatial beam characteristics; moreover, we will consider that the pulse propagates through a linear optical system without gain or losses.

The complex electric field in the time domain of a signal travelling in the z -direction is

$$U(z = 0, t) = A(z = 0, t) \exp [i2\pi\nu_0 t], \quad (1)$$

where ν_0 is the carrier frequency and $A(z, t)$ is the complex field envelope. For the smoothest variant envelope, ν_0 , corresponds to the mean frequency.

In order to evaluate the propagation of a pulse through an optical system, it is necessary to study the response to each temporal frequency and to reconstruct the pulse from the output frequency spectrum. The necessary tool for time-to-frequency conversion is the temporal Fourier transform, that will be identified by the symbol $\hat{\cdot}$. In this way, the input spectrum of the signal is

$$\begin{aligned} \hat{U}(0, \nu) &= \int_{-\infty}^{\infty} U(0, t) \exp[-i2\pi\nu t] dt \\ &= \hat{A}(0, \nu - \nu_0) = \hat{A}(0, \nu'), \end{aligned} \quad (2)$$

where $\hat{A}(0, \nu)$ is the frequency spectrum of $A(0, t)$.

A linear optical system is characterized by a complex optical transfer function, $H_S(\nu) = R(\nu) \exp[-i\Psi(\nu)]$, that relates the input and output field spectrum. Then, the output field at a distance z is

$$\hat{U}(z, \nu) = \hat{U}(0, \nu) H_S(\nu). \quad (3)$$

In this section, to get an insight of how the phase response affects the pulse, we assume that the amplitude response of the system, $R(\nu)$, does not change over the pulse spectrum and that it is equal to one. If the phase variation differs from the distortionless case (linear phase), it can be characterized, for narrowband signals having frequency components primarily near the carrier frequency ν_0 , through a Taylor expansion,

$$\begin{aligned} \Psi(\nu) &= 2\pi \sum_{n=0}^{\infty} \frac{b_n}{n!} \nu^n, \quad \text{where} \\ b_n &= \frac{1}{2\pi} \left. \frac{d^n \Psi(\nu)}{d\nu^n} \right|_{\nu_0}. \end{aligned} \quad (4)$$

Thus, the output complex field is

$$\begin{aligned} U(z, t) &= \int_{-\infty}^{\infty} \hat{U}(z, \nu) \exp[i2\pi\nu t] d\nu \\ &= A(z, t) \exp[i2\pi\nu_0 t] \exp[-i\Psi(\nu_0)], \end{aligned} \quad (5)$$

where $A(z, t)$ is the inverse time Fourier transform of $\hat{A}(z, \nu') = \hat{A}(0, \nu') H(\nu')$. Here, $H(\nu')$ is the temporal transfer function of the complex envelope given by

$$\begin{aligned} H(\nu') &= \exp \left[-i2\pi \sum_{n=1}^{\infty} \frac{b_n}{n!} \nu'^n \right] \\ &\approx \exp[-i2\pi t_g \nu'] \exp[-i\pi D \nu'^2], \end{aligned} \quad (6)$$

with $t_g = b_1$ being the group delay and $D = b_2$ the dispersion coefficient. If D is sufficiently small, it may also be neglected. Then the system implements simply a delay of the complex envelope without altering its shape. However, depending on the signal and system characteristics, the quadratic spectral phase also needs to be considered. Its non-zero value indicates that the delay of the signal varies over the bandwidth of interest and provokes a change in the envelope shape. In our theoretical description we neglect higher-order expansion coefficients that also change the pulse envelope and chirp.

3. The Montgomery interferometer as a temporal device

In this section, we apply the previous mathematical formalism to the Montgomery interferometer. For the mathematical description, we consider 1D Montgomery objects, assuming that the material dispersion of the substrate of the diffractive element is negligible.

Montgomery showed that, under monochromatic plane-wave illumination of $\lambda_0 = c/\nu_0$, the diffracted field generated by a 1D object will periodically self-image with a longitudinal period z_M if its angular spectrum is reduced to a discrete set of frequencies given by

$$\rho_m = \sqrt{\left(\frac{\nu_0}{c}\right)^2 - \left(\frac{m}{z_M}\right)^2}, \quad m = 1, 2, 3, \dots, m_{\max}. \quad (7)$$

The Montgomery interferometer is shown in Fig. 2. It is constituted by two phase-complementary objects, $M_{i=1,2}(x)$, that satisfy Eq. (7). The diffracting objects are separated by a multiple of z_M , $z = Mz_M$. Although this last assumption is not always required, it improves the efficiency of the system.

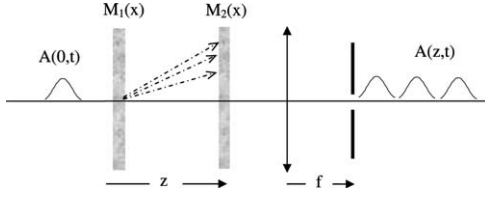


Fig. 2. Schematic diagram of the Montgomery interferometer as a time filter.

Let us denote by (u_x, u_y) the spatial frequencies. The diffracting screen spatial spectrum is obtained after performing a spatial Fourier transform, indicated by the tilde symbol \sim , over the amplitude distribution of the object,

$$\begin{aligned} \tilde{M}_1(u_x, u_y) &= \int_{-\infty}^{\infty} M_1(x) \exp [i2\pi(u_x x + u_y y)] dx dy \\ &= \sum_m C_m \delta(u_x - \rho_m) \delta(u_y) \end{aligned} \quad (8a)$$

and

$$\begin{aligned} \tilde{M}_2(u_x, u_y) &= \int_{-\infty}^{\infty} M_2(x) \exp [i2\pi(u_x x + u_y y)] dx dy \\ &= \sum_n C_n^* \delta(u_x + \rho_n) \delta(u_y). \end{aligned} \quad (8b)$$

When $M_1(x)$ is illuminated by the pulsed plane wave given by Eq. (1), the input spectrum of the signal is

$$\hat{U}_1^-(z=0, \nu) = \hat{A}(z=0, \nu') \delta(u_x) \delta(u_y), \quad (9)$$

where $\nu = \nu' + \nu_0$. Immediately behind the mask

$$\hat{U}_1^+(0, \nu) = \sum_m C_m \hat{A}(0, \nu') \delta(u_x - \rho_m) \delta(u_y). \quad (10)$$

Next, we consider free-space signal propagation over a distance $z = Mz_M$ with $M = 1, 2, 3, \dots$. We restrict ourselves to the validity of the scalar diffraction theory, where the propagation is a linear and shift-invariant system whose transfer function over a distance z is

$$\begin{aligned} H_{F-S}(u_x, u_y, \nu) &= \exp \left[-i2\pi \sqrt{\left(\frac{\nu}{c}\right)^2 - u_x^2 - u_y^2} z \right] \\ &\text{valid for } u_x, u_y < \frac{\nu}{c}. \end{aligned} \quad (11)$$

The last assumption is a physical restriction for the system because for higher spatial frequencies the propagation is carried by evanescent waves.

Consequently, before $M_2(x)$, the complex field is provided by

$$\begin{aligned} \hat{U}_2^-(z, \nu) &= \sum_m C_m \hat{A}(0, \nu') \delta(u_x - \rho_m) \delta(u_y) \\ &\times \exp \left[-i2\pi \sqrt{\left(\frac{\nu}{c}\right)^2 - \rho_m^2} z \right], \end{aligned} \quad (12)$$

and behind it, the spectral distribution is

$$\hat{U}_2^+(z, \nu) = \hat{U}_2^-(z, \nu) \otimes \tilde{M}_2(u_x, u_y), \quad (13)$$

where the symbol \otimes means convolution. After some straightforward calculations, the output field of the Montgomery interferometer is

$$\begin{aligned} \hat{U}_2^+(z, \nu) &= \sum_m |C_m|^2 \hat{A}(0, \nu') \delta(u_x) \delta(u_y) \\ &\times H_{F-S}(u_x = \rho_m, u_y = 0, \nu) + \sum_m \sum_{n \neq m} C_m C_n^* \hat{A}(0, \nu') \\ &\times \delta(u_x - \rho_m + \rho_n) \delta(u_y) H_{F-S}(u_x = \rho_m, u_y = 0, \nu). \end{aligned} \quad (14)$$

We are interested in the output on-axis plane wave, which corresponds to the case where $n = m$. Physically, this can be achieved by selecting the zeroth order of the spatial Fourier transform of the output distribution with the aid of a refractive lens, see Fig. 2. Then, the second sum in Eq. (14) can be removed and the transfer function of the system takes the form

$$H_s(\nu) = \sum_m |C_m|^2 \exp \left[-i2\pi \sqrt{\left(\frac{\nu}{c}\right)^2 - \rho_m^2} z \right]. \quad (15)$$

Therefore, the output pulse characteristics can easily be determined by multiplying the field spectrum of the incident pulse with Eq. (15). Notice that for each spatial frequency of the first mask, the effect caused by the Montgomery interferometer is an amplitude response that depends on the design coefficients of the Montgomery object and a temporal frequency-variant phase response that corresponds its free space propagation. Observe that every one of the phase responses differs from the ideal linear function. This fact

justifies performance of a Taylor expansion to each phase of the sum and the use of bandwidth-limited signal.

When all the terms in Eq. (15) have a linear phase, according to the theory developed in Section 2, each phase shift provides a group delay given by

$$t_g^m = \frac{1}{2\pi} \left. \frac{d\Psi(v)}{dv} \right|_{v_0} = \frac{v_0 z}{c^2 \sqrt{\left(\frac{v_0}{c}\right)^2 - \rho_m^2}}, \quad (16)$$

or after the substitution of Eq. (7)

$$t_g^m = \frac{Mz_M^2 v_0}{c^2 m} = \frac{v_0 m M}{c^2 \left(\left(\frac{v_0}{c}\right)^2 - \rho_m^2\right)}, \quad (17)$$

where the superindex m is used to emphasize the fact that for each spatial frequency, we obtain a different delay.

In the paraxial approximation of the diffraction theory and when $\rho_n = \sqrt{n}\rho_1$, the Montgomery distance is given by $z_M = 2v_0/\rho_1^2 c$ and

$$t_g^n = \frac{Mz_M}{c} + M \frac{nz_T \rho_1^2 c}{2v_0^2} = t_g^{n=0} + M \frac{n}{v_0}, \quad (18)$$

$n = 0, 1, 2, 3, \dots$

Notice that, in this case, there is a linear dependence of the group delay on the index n .

In the linear phase approximation, the transfer function of the complex envelope is

$$H(v') = \sum_k |C_k|^2 \exp \left[-i2\pi t_g^k v' \right], \quad (19)$$

with k being m or n , and the complex envelope in the temporal domain is

$$\begin{aligned} A(z, t) &= A(0, t) \otimes \sum_k |C_k|^2 \delta(t - t_g^k) \\ &= \sum_k |C_k|^2 A(0, t - t_g^k). \end{aligned} \quad (20)$$

From Eq. (20), we conclude that under the second-order approximation, the setup can be used as a pulse train generator or as transversal filter (see Fig. 1). If the delay time between two consecutive pulses is larger than the duration of the pulse, we will obtain a train of pulses. On the other hand, if the delay is shorter, the output is determined by their superposition. This latter case corresponds to a transversal filter for which the calculation of the

tap delays the trivial shift z/c due to propagation must be omitted.

Now, we continue with the third-order approximation of the phase function. The dispersion coefficient for each phase term of Eq. (15) is

$$D^m = \frac{1}{2\pi} \left. \frac{d^2\psi(v)}{dv^2} \right|_{v_0} = \frac{b_{1m}^M \rho_m^2 c^2}{(c^2 \rho_m^2 - v_0^2) v_0}. \quad (21)$$

Thus, the transfer function of the envelope takes the form

$$H(v') = \sum_m |C_m|^2 \exp \left[-i2\pi t_g^m v' \right] \exp \left[-i\pi D^m v'^2 \right], \quad (22)$$

and the time-domain output complex envelope is

$$A(z, t) = \sum_m |C_m|^2 A(0, t - t_g^m) \otimes \exp \left[i \frac{2\pi}{D^m} t^2 \right]. \quad (23)$$

Eq. (23) can be interpreted as a temporal filter over a delay version of the envelope. When the time delay is bigger than the pulse duration, it guarantees the ability of the setup to perform a different pulse-shaping to each pulse of the train. Also, for single-spatial frequency Montgomery objects, it is easy to demonstrate that the device reduces to the Treacy grating-pair compressor.

To complete this section, we would like to make a short remark about the Talbot interferometer. The heart of the Talbot interferometer as a time filter [12] lies in the same theoretical background as for the Montgomery interferometer and can also be considered as a particular case. In fact, 1D gratings of period p are a subgroup of Montgomery objects with spatial frequencies $\rho_n = n/p$ and a separation between to self-images of $z_T = 2p^2 v_0/c$. Therefore, all the theory developed for the Montgomery interferometer is also applicable to the Talbot interferometer by performing these small changes.

4. Numerical examples

In the previous section, we have studied the temporal transfer function of the Montgomery interferometer. Now, we present some numerical

results that may help provide a complete information and understanding of the system.

For some of the examples, we will consider a Ti:sapphire laser producing pulses at a mean frequency $\nu_0 = 361$ THz ($\lambda_0 = 830$ nm) and a Montgomery distance of $z_M = 22$ mm. Fig. 3(a) shows the phase transfer function for two individual spatial frequencies. The solid curve is valid for $\rho_m = 0.488 \mu\text{m}^{-1}$ which corresponds to $m = 24, 200$ and the dashed line for $\rho_m = 0.323 \mu\text{m}^{-1}$ calculated with $m = 25, 500$. The selection of these spatial frequencies is arbitrary just to study the different behaviour of the system for low or high spatial frequencies. Fig. 3(b) shows the frequency-dependent delay of this configuration defined as

$$\tau(\nu) = \frac{1}{2\pi} \frac{d\Psi(\nu)}{d\nu}. \quad (24)$$

From these graphs we can decide whether the second- or third-order term in the approximation of each individual phase is valid for each spatial frequency depending on the spectrum of the source. If the group delay is constant over the spectral range of interest, a second-order approximation will be enough, but in other cases at least a quadratic approximation is needed.

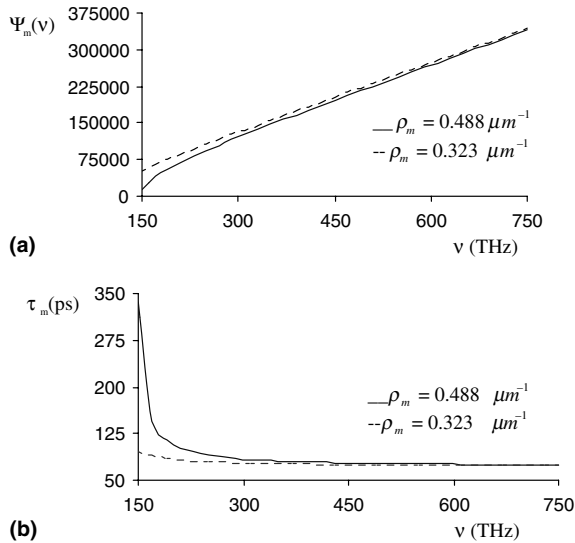


Fig. 3. Graphs of the: (a) phase transfer function and (b) group delay obtained for two different spatial frequencies with ν_0 THz and $z_M = 22$ mm.

Next, we check that the system configuration works properly under the approximations suggested in the previous section. In a Taylor series of a function $\Psi(\nu)$ up to order n in the surrounding of a point ν_0 , R_n is a remainder term known as the Lagrange remainder, which is given by

$$R_n = \frac{(\nu - \nu_0)^{n+1}}{(n+1)!} \left. \frac{d^{n+1}\Psi(\nu)}{d\nu^{n+1}} \right|_{\nu=e}, \quad (25)$$

so the maximum error after n terms of the Taylor series is the maximum value of Eq. (25) running through all $e \in [\nu, \nu_0]$. We define a figure of merit, F_n^m , that quantifies the error of the approximation till order n by considering that the last term of the Taylor expansion must be much greater than the Lagrange remainder

$$F_n^m = \left| \frac{R_n n!}{2\pi b_n \Delta \nu^n} \right| \ll 1, \quad (26)$$

where $\nu - \nu_0$ has been approximated to the spectral width of the pulse $\Delta \nu$ measured in the full width at half maximum (FWHM). As an example, Fig. 4 shows the dependence of F_1^m on the three parameters that affect its behaviour: the spatial frequency, the carrier frequency and the bandwidth of the pulse. For this case $e = \nu_0 - \Delta \nu$. By increasing the spatial frequency or the bandwidth of the pulse, the value of F_1^m will also increase. On the other hand, an increment of the carrier frequency will cause a reduction of the merit function. Similar graphs can be obtained, F_2^m , for those setups where the second-order approximation is clearly not sufficient.

Now as a numerical example, we study the formation of a sequence of two pulses. We implement a Montgomery object with two spatial frequencies $\rho_1 = 0.005 \mu\text{m}^{-1}$ and $\rho_5 = 0.011 \mu\text{m}^{-1}$. The low frequencies chosen allow us to consider the paraxial approximation where the delay between two consecutive pulses has a linear relation with the order of the spatial frequency n , see Eq. (18). As a source we use the previously mentioned Ti:sapphire laser producing pulses of a duration $\Delta t = 87$ fs. To calculate the bandwidth of the signal, we can use the expression

$$\Delta \nu \Delta t \geq 0.441, \quad (27)$$

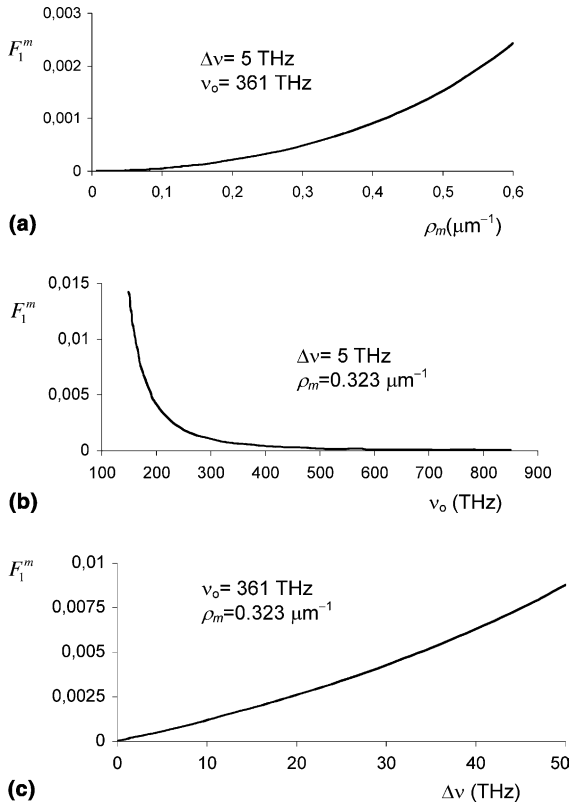


Fig. 4. Graphs of the merit function for the second-order approximation in relation of: (a) the spatial frequency, (b) the carrier frequency and (c) the bandwidth of the pulse.

which relates the bandwidth and the duration of Gaussian shape pulses when both quantities are measured at the FWHM [23]. The equal sign in Eq. (27) yields a bandwidth of $\Delta\nu = 5$ THz. We chose $z_M = 2\nu_o/\rho_m^2 c = 96$ mm and $M = 15$. Consequently, we obtain two output pulses delayed by $t_g^{n=5} - t_g^{n=1} = 166$ fs. Comparing this number with the value for the pulse duration may show the usefulness of the device as a pulse train generator. Currently work is ongoing, where these simple considerations will be extended by numerical techniques and compared with experimental results.

5. Conclusions

A theoretical description of the Montgomery interferometer based on the concept of the transfer

function was given. It describes the operation of the interferometer for on-axis plane waves as the input and the output signals. Due to the spatio-temporal coupling, the temporal transfer function is mainly the weighted sum of the transfer function of free-space propagation for each spatial frequency of the first Montgomery object. We also showed that each individual phase term of transfer function suffers from distortion, but for relatively narrowband signals they can be approximated by the first two or three terms of a Taylor series expansion.

In this way, when each phase term has a linear behaviour with the temporal frequency, the setup is suitable for the implementation of a tapped delay-line filters and for the generation of equal shape pulses. We also showed that under the quadratic approximation of the phase, the shaping of the each output envelope is described by its dispersion coefficient. Then, it is possible to generate a sequence of pulses where each pulse has a different envelope.

Finally, we defined a merit function that considers the goodness of the Taylor approximation and we presented, as a first example of the potential application of the system, some numerical data calculation related to the generation of a pair of pulses. Theory and simulated results demonstrate the validity of the Montgomery interferometer for temporal processing.

Acknowledgements

This work was done at the Optische Nachrichtentechnik-group at the FernUniversität Hagen (Germany). G. Mínguez-Vega gratefully acknowledges financial support from the Generalitat Valenciana, Agencia Valencia de Ciencia y Tecnología (grant CTESPP/2003/068). The authors appreciate useful discussions with Adolf W. Lohmann and Hans Knuppertz.

References

- [1] H.F. Talbot, *Philos. Mag.* 9 (1836) 401.
- [2] W.D. Montgomery, *J. Opt. Soc. Am.* 57 (1967) 772.

- [3] K. Patorski, in: E. Wolf (Ed.), *Progress in Optics*, vol. 27, North-Holland, Amsterdam, 1989.
- [4] A. Lohmann, in: K.J. Habbell (Ed.), *Proceedings of the ICO Conference on Opt. Instr.*, London, 1961, p. 58.
- [5] H.L. Kung, A. Bhatnagar, D.A.B. Miller, *Opt. Lett.* 26 (2001) 1645.
- [6] E. Tajahuerce, E. Bonet, J. Lancis, M.T. Gale, P. Andres, *J. Mod. Opt.* 48 (2001) 831.
- [7] M. Gruber, D. Hagedorn, W. Eckert, *Appl. Opt.* 40 (2001) 5052.
- [8] A.W. Lohmann, D.E. Silva, *Opt. Commun.* 9 (1971) 413.
- [9] G. Indebetouw, *Opt. Acta* 30 (1983) 1463.
- [10] S. Sinzinger, J. Jahns, *Microoptics*, Wiley-VCH, Weinheim, 2003.
- [11] J. Jahns, H. Knuppertz, A.W. Lohmann, *Opt. Commun.* 225 (2003) 13.
- [12] J. Jahns, E. ElJoudi, D. Hagedorn, S. Kinne, *Optik* 112 (2001) 295.
- [13] K. Sasayama, M. Okuno, K. Habara, *Electron. Lett.* 25 (1989) 1508.
- [14] R.J. Berinato, *Appl. Opt.* 32 (1993) 5797.
- [15] D.B. Hunter, R.A. Minasian, *Electron. Lett.* 31 (1995) 1010.
- [16] K. Okamoto, H. Yamada, T. Goh, *Electron. Lett.* 35 (1999) 1331.
- [17] C.K. Madsen, J.H. Zhao, *Optical Filter Design and Analysis*, Wiley, New York, 1999.
- [18] A.W. Weiner, *Rev. Sci. Instrum.* 71 (2000) 1929.
- [19] F.G. Omenetto, in: E. Wolf (Ed.), *Progress in Optics*, vol. 44, North-Holland, Amsterdam, 2002.
- [20] C. Froehly, B. Colombeau, M. Vampouille, *Shaping and analysis of picosecond light pulses*, in: E. Wolf (Ed.), *Progress in Optics*, vol. 20, 1983.
- [21] E.B. Treacy, *IEEE J. Quantum Electron.* 5 (1969) 454.
- [22] A.M. Weiner, J.P. Heritage, E.M. Kirschner, *J. Opt. Soc. Am. B* 5 (1988) 1563.
- [23] J.-C. Diels, W. Rudolph, *Ultrashort Laser Pulse Phenomena*, Academic Press, San Diego, 1996.
- [24] B.E.A. Saleh, M.C. Teich, *Fundamentals of Photonics*, Wiley, New York, 1991.